Author's personal copy

Chemical Engineering Science 64 (2009) 560 – 567

Contents lists available at ScienceDirect

Chemical Engineering Science

journal homepage: www.elsevier.com/locate/ces

Catalytic nanoliths

H. Feng[d], J.W. Elam[b], J.A. Libera[b], M.J. Pellin[c], P.C. Stair[a,d,*]

[a]Department of Chemistry and Center for Catalysis and Surface Science, Northwestern University, Evanston, IL 60208, USA
[b]Energy Systems Division, Argonne National Laboratory, Argonne, IL 60439, USA
[c]Materials Science Division, Argonne National Laboratory, Argonne, IL 60439, USA
[d]Chemical Sciences and Engineering Division, Argonne National Laboratory, Argonne, IL 60439, USA

ARTICLE INFO

Article history:
Received 20 April 2008
Received in revised form 16 September 2008
Accepted 17 September 2008
Available online 17 October 2008

Keywords:
Catalysis
Nanostructure
Porous media
Multiphase reactions
Anodic aluminum oxide (AAO)
Oxidative dehydrogenation (ODH)

ABSTRACT

The nanoporous anodic aluminum oxide (AAO) structure is shown to be a useful platform for heterogeneous catalysis. By appropriately masking the perimeter during anodization and etching, the AAO can be formed at the center of an aluminum disc. The remaining aluminum ring connects seamlessly to the AAO and provides mechanical support for convenient handling. The supported AAO can be sealed in a standard fitting so that the nanopores in the structure function as an array of tubular reactors, i.e. a nanolith. Coating the walls with catalytically active materials turns the nanolith into a novel catalytic system. For the oxidative dehydrogenation (ODH) of cyclohexane, the nanolith catalytic system is superior to a conventional powdered catalyst in terms of both efficiency and in reducing over oxidation. A simple analysis of the flow through the nanolith combined with experimental data indicates that mass transfer through the nanopores follows a mixed flow model.

© 2008 Elsevier Ltd. All rights reserved.

1. Introduction

Porous anodized aluminum oxide (AAO) structures feature a highly ordered array of straight nanopores (Patermarakis and Pavlidou, 1994; Masuda and Fukuda, 1995). For the last half a century this material has been widely used as micro-filters, anti-corrosion barrier layers, and as substrates for various coatings (Kuo and Xu, 2006; Kyotani et al., 2002; Tomioka and Yoshida, 2001). In recent years, AAO structures have found application in the nanofabrication field because the ordered nanopores form an ideal template for synthesizing a variety of nanostructures (Martin, 1994; Masuda et al., 1995, 1997; Gao et al., 2002). However, the application of AAO structures as a framework for catalysts remains an intriguing but little investigated area. The functionality of a heterogeneous catalyst depends critically on its structure over a range of length scales (Goodwin et al., 2004; Weitkamp et al., 1999). At the length scale of 10s–1000s of nanometers, the dimensions and topology of the catalyst pore structure can influence reagent flow, the sequencing of catalytic active sites, and the contact time between reagents and catalyst (Roy et al., 2003). Conceptually, the AAO structure consists of an assembly of identical pores having nanometer dimensions that span a flow reactor so as to produce an array of nanoreactors that we call the *catalytic nanolith*, i.e. a nanometer scale version of the catalytic monolith. With this assembly, each reagent molecule must traverse an identical pore and, ideally, each diffusion path can be engineered through control over the pore diameter, wall composition, and length. This results in more uniform and tunable contact times than are possible with a conventional fixed bed powder catalyst.

Besides fine control over diffusion paths and contact times, this catalytic system also provides a number of additional possibilities. For example, its open, one-dimensional channel structure facilitates the deposition of coatings and catalytically active materials. One good example is the application of atomic layer deposition (ALD) in fabricating a catalytically active nanolith. Traditionally this powerful deposition technique has been used in the coating of flat surfaces; its application in the catalysis field can be limited by diffusion into powder supports with very small irregular pores (McCormick et al., 2007). In our studies, ALD has been shown to be a powerful tool for adjusting the pore size, controlling chemical composition, and synthesizing interesting catalytic structures inside the AAO nanopores (Stair et al., 2006). Another feature of this nanolith catalytic system is the possibility to study the influence of reagent delivery on catalytic performance. For example, with an asymmetric reactor it is possible to deliver two reagents on opposite sides of the nanolith structure or to sweep reactants or products away from the entrance and exit of the structure (as pictured in Fig. 1(a)) in order to control the flow of molecules that enter and exit the nanolith. Catalytic results from such experiments may be a valuable test of theoretical predictions regarding the location of catalytic transformations in the

* Corresponding author at: Department of Chemistry and Center for Catalysis and Surface Science, Northwestern University, Evanston, IL 60208, USA.
E-mail address: pstair@northwestern.edu (P.C. Stair).

0009-2509/$ - see front matter © 2008 Elsevier Ltd. All rights reserved.
doi:10.1016/j.ces.2008.09.027

Author's personal copy

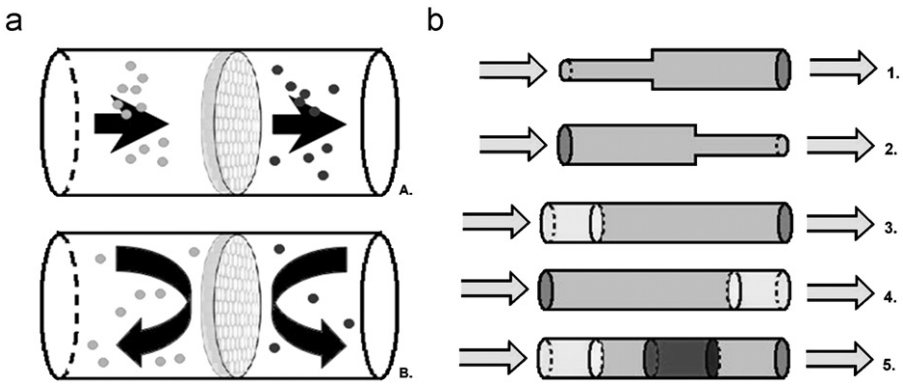

Fig. 1. (a) The push-through flow mode (A) and the sweep flow mode (B) in a nanolith reactor. (b) Different pore structures and catalysts locations (the different shading represents the regions where different catalytically active materials are coated on the pore wall): asymmetric pore diameters (1 and 2); catalyst located near the entrance (3) and the exit (4); controlled sequence of different catalysts along the pore (5).

pores (Albo et al., 2006). Furthermore, the influence of the flow pattern in the nanopores on the catalytic performance can also be studied. Using ALD, the sizes and shapes of the nanopores can be finely tuned. The pore diameter can be adjusted in the range of 2–40 nm (using a 40 nm pore AAO as the starting point) with Ångstrom scale precision. By controlling the preparation conditions, it is even possible to synthesize asymmetric nanoliths with pores of different diameters and compositions open on the two sides (Li et al., 1999). Since the dimensions of the nanopores significantly influence the flow pattern of the reagents inside the pores, a measure of control over the catalytic properties of the nanolith system can be achieved (Albo et al., 2006). We can also investigate how the spatial location of the catalytically active materials in the pores influences the catalytic performance. For example, it is possible, using ALD diffusion techniques, to locate the catalytic material at the entrance or exit to the pores or even to arrange the catalytic material as a series of bands down the length of the pore. Similarly, the formation of a controlled sequence of different catalytic materials is a topic of interest. Schematic pictures of some catalytic structures of interest are depicted in Fig. 1(b).

The arrays of nanoreactors on the AAO structure make a promising, highly selective catalytic system for some sequential reactions. When the reactants flow through the nanolith, the limited fraction of the pore length and precise position over which the catalytic film is deposited may dramatically reduce the contact time between reactants and catalyst so that undesirable over reactions can be limited to a great extent. The oxidative dehydrogenation (ODH) of alkanes to olefins is a sensitive probe for the performance of the nanolith because the partial oxidation products are easily oxidized to oxygenated products, which are thermodynamically more stable (Corberan, 2005; Mamedov and Corberan, 1995; Kung, 1994). The ODH of cyclohexane catalyzed by supported vanadium oxides is an example, in which cyclohexane is first converted to cyclohexene and then further oxidized to benzene and oxygenated products such as CO and CO_2. In this reaction it is difficult to achieve a high yield of cyclohexene as the partial oxidation product (Panizza et al., 2003). In our earlier work we have reported that VO_x supported on the AAO structure exhibits much better performance than a conventional vanadia powder in terms of the selectivity to cyclohexene (Stair et al., 2006). However, those experiments were carried out in a reactor system where the AAO structures were not sealed to the reactor walls. In that configuration, bypass of the reactant around the catalyst is inevitable. This motivated the desire to study the sealed, gas-tight AAO structure in a flow reactor, in which the reactant is forced to flow through the nanopores, forming a nanolith. However, due to the fragile nature of this ~100 μm thick material, little sealing force can be directly applied without breaking the AAO. Our solution to this problem is to mount the AAO structure onto a supporting material that can accept the force of the seal in a conventional gas-tight fitting.

In this paper we report a novel method of synthesizing an AAO structure embedded in an aluminum ring support. The concept of the nanolith is realized by sealing the AAO in a flow reactor adapted from a standard Swagelok VCR fitting so that the reactants must flow through the nanopores. The performance of the nanolith catalytic system is compared to that of a powder bed for the ODH of cyclohexane catalyzed by supported vanadium oxides. The performance of the nanolith is analyzed using a physical model that includes factors such as the mass flow, diffusion, and the chemical reactions inside the nanopores.

2. Experimental

To prepare an AAO structure embedded in an aluminum ring support, a Teflon holder was designed to mask part of the aluminum surface during anodization (Fig. 2(a) and (b)). The holder is made of two pieces of Teflon, between which rests the aluminum disk of the desired size. In our case this is 18 mm to allow insertion in a standard VCR fitting. On one piece of Teflon (the front piece) a hole is drilled in the center (I.D. = 9 mm) so that the central region on one side of the aluminum disc is exposed. The back Teflon plate has threaded screw holes so that the two plates can be tightly held together using Teflon screws. Two Viton O-rings of different sizes are used to provide firm seals so that *only* the central, front-side region of the aluminum disk is in contact with the electrolyte. Viton was chosen in order to prevent the degradation of the O-ring support directly exposed to the oxalic acid solution. Electrical contact to the back side of the aluminum disk is established by a copper cup via a metal screw that passes along in a hole in the back piece of Teflon plate. During anodization or etching, the top portion of the holder is held above the surface of the liquid so that the metal screw and copper cup remain dry.

The method of growing the AAO structure follows well-established procedures (Masuda and Fukuda, 1995). Cleaned and electro-polished aluminum sheets (99.99%, Alfa Aesar) were cut into disks that fit into the anodization holder. These discs were anodized for 24 h in a 0.3 M oxalic acid solution at a constant potential of 40 V at 3 °C. The AAO structures prepared under these conditions are 70 μm thick and have an average pore diameter of about 40 nm. A standard two-step anodization procedure was applied to ensure that a highly ordered hexagonal pattern of pores was formed. After the anodization, the un-anodized back side of the aluminum

Author's personal copy

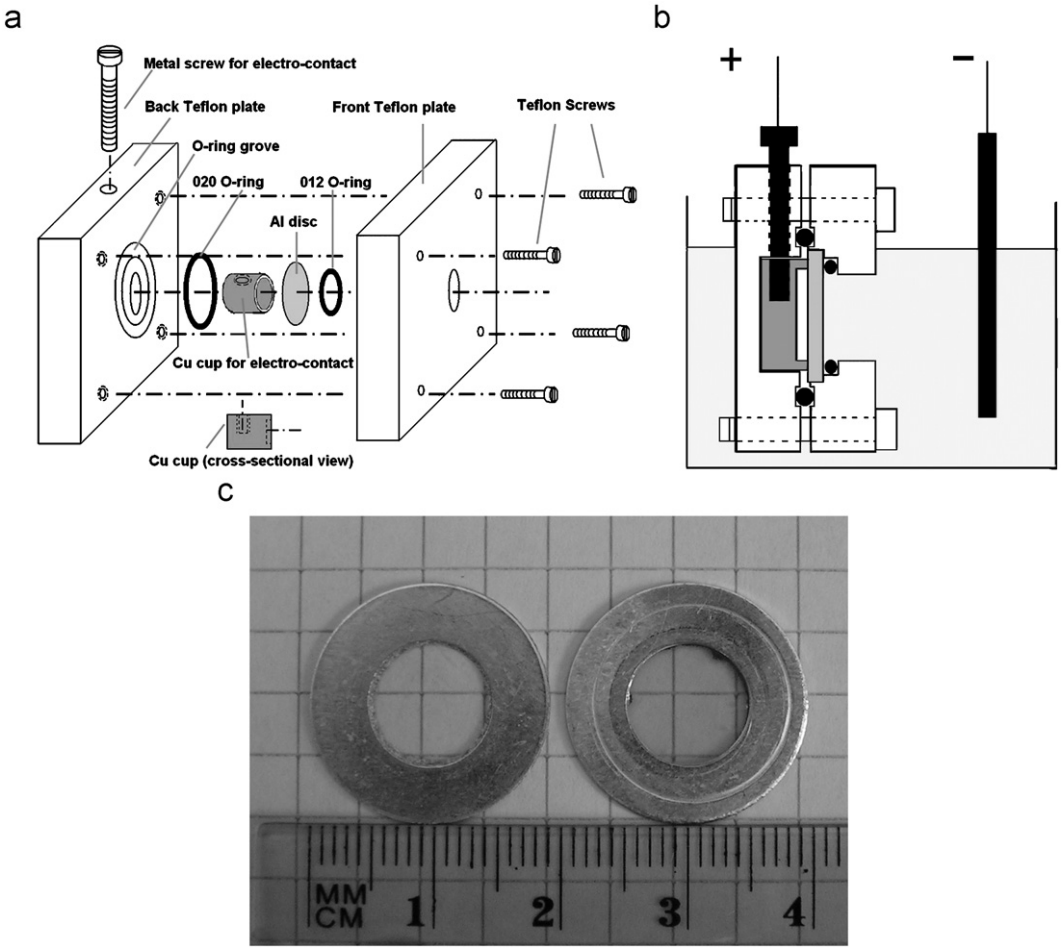

Fig. 2. (a) The dissembled anodization cell. In this fixture a metal screw penetrates a clearance hole parallel to the face of the back Teflon plate and screws into the copper cup (with the threaded screw hole). The copper cup makes electrical contact to the aluminum disc. Four Teflon screws penetrate the front Teflon plate and screw into the back Teflon plate with threaded holes. (b) Anodization on one side of the aluminum disc. (c) A photo of the AAOs/aluminum ring supports. The AAO structure on the left is an as-prepared nanolith. The AAO structure on the right is the one after ALD VO_x coating and cyclohexane ODH catalysis testing. The darker (light yellow) color on the right piece of AAO is from the ALD VO_x; the grove on the aluminum ring is due to sealing in the VCR fitting.

disk (except for the supporting ring) was dissolved in 37% HCl/10% $CuCl_2$ ($\frac{1}{4}$ v/v) solution. In this step, the disk is turned around in the Teflon holder to etch the aluminum and expose the bottom of the AAO structure. This back side of the AAO structure was treated in 5% phosphoric acid at 30 C° for 70 min to remove the barrier layer on the bottom of the AAO structure so that both ends of the channels were open. A photograph of the AAO structure embedded in the aluminum ring, as prepared (left) and after ALD VO_x catalyst loading and cyclohexane ODH catalysis testing (right) is shown in Fig. 2(c). The synthesized AAO has an I.D. of about 9 mm, which is determined by the size of the inner O-ring. The durability of these fragile AAOs is greatly enhanced by the supporting aluminum ring. A rather wide (~4.5 mm) aluminum ring support makes it convenient to seal the AAO structure in a Swagelok VCR fitting and helps reduce the tension transferred to the AAO when the aluminum ring is deformed on sealing. The surface topology and structure of the AAO materials were studied with a Hitachi S4700 SEM.

Before loading catalytic materials onto the as-prepared nanolith, approximately 1 nm of Al_2O_3 was coated onto the AAO by ALD to completely cover electrolyte impurities incorporated into the oxide material during anodization. Alumina ALD was carried out at 200 °C in a viscous flow reactor (Elam et al., 2002; Stair et al., 2006). Ultra-high purity nitrogen was used as the purge gas. The layer-by-layer growth of alumina was achieved by alternatively exposing the AAO substrates to trimethyl aluminum and water for eight cycles using a quasi-static reactor operation mode in which the reactor is pumped down to 0.1 Torr after each dose and purge. Dosing was done statically by closing the exhaust valve and then filling the reactor at 0.1 Torr with pure reagent (trimethyl aluminum or H_2O) to 1 Torr and then holding for 5 s. The purge cycle was a continuous flow of 300 sccm of N_2 at 1 Torr for 20 s. The alumina layer also serves to cover any exposed aluminum metal with the same oxide structure and composition as the rest of the nanolith ensuring that catalytic reactants are exposed to a uniform material. Vanadium oxide catalytic material (VO_x) was then introduced by ALD using a procedure similar to that reported by Keranen et al. (2004), in which the AAO was exposed to vanadyl oxytriisopropoxide and hydrogen peroxide/water. A dosing/purging timing sequence of 45–30–45–30 s was used to deposit layer(s) of VO_x onto the AAO structure at 100 °C, 1.1 Torr, with a nitrogen flow rate of 240 sccm/min.

Catalytic reactions were performed in an ALD-alumina-coated stainless steel reactor modified from a standard Swagelok VCR fitting, in which the gasket was replaced by the nanolith system. The empty space in the reactor was filled with quartz chips to minimize gas phase reactions (Kung, 1994). A small amount of Quartz wool was used to hold the quartz chips and to provide a separation between the quartz chips and the nanolith. A schematic picture of the reactor setup is depicted in Fig. 3. Cyclohexane vapor was introduced into

Author's personal copy

the reaction system using a helium bubbler. Pure oxygen was used as the oxidant, and helium was used as the diluent. The reactant gas was made up of 1% cyclohexane, 2% oxygen, and 97% helium. The total flow rate through the reactor was 10 sccm/min. The oxidation reaction was carried out at temperatures between 400 and 480 °C at atmospheric pressure. The reaction products were analyzed with an HP 6890 gas chromatograph equipped with FID and TCD detectors.

3. Results and discussion

A gas-tight seal between the nanolith system and the flow reactor is required to ensure that the reactants must flow through the nanopores and gas bypass is eliminated. With our assembly a crack or gap at the boundary between the AAO and the supporting aluminum ring is the most likely location for gas bypass. Therefore this region was examined with SEM. As seen in Figs. 4 and 5, the morphology of the boundary regions on the front side (the anodized side) looks quite different from the back side (the etched side). On the front side, the AAO layer becomes thinner as it approaches the edge; at the boundary an alumina layer of several microns thick joins the aluminum on the ring. In this boundary region, aluminum can be found buried under the thin layer of AAO. Additionally, the pattern of the pores near the front side edge is not as regular as that in the center of the nanolith. On the back side, however, the actual boundaries seem to be completely covered by the aluminum and there is no noticeable difference in the regularity of the pores between the edge and the center of the AAO. Generally speaking, the transition from AAO to aluminum ring support is seamless; there is no evidence of cracking along the AAO/aluminum boundary. Based on the above observations, a schematic picture of the cross-sectional view of the connection between the AAO structure and the aluminum ring is drawn in Fig. 6. Remarkably this transition region is quite narrow representing less than 5% of the total surface area of the nanolith.

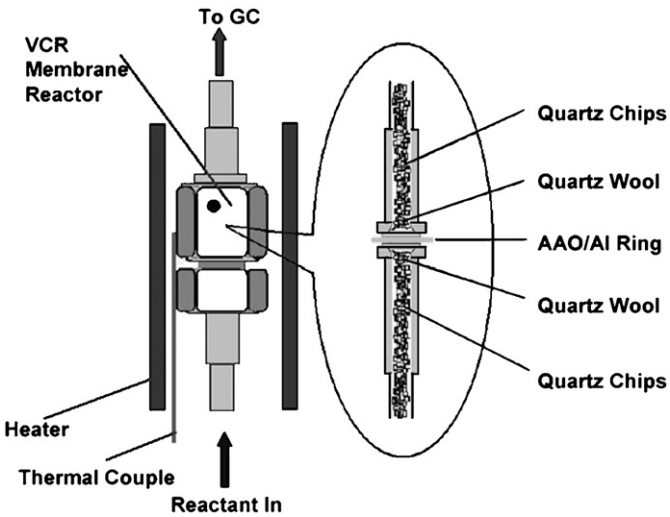

Fig. 3. Schematic picture of the nanolith reactor setup.

The nanolith can be sealed in a standard Swagelok face seal adaptor (VCR fitting), in which two metal glands are tightly held against the aluminum ring to form a gas-tight seal (see Fig. 7). The adaptor is carefully fastened until no leak can be detected as flowing gas is purged through the fitting. A pressure drop due to the resistance of the nanopores to the flow of gas is present across the nanolith, which serves as an indicator of structural integrity. This pressure drop is related to the size and shape of the nanopores and the density, viscosity, and flow rate of the gas. Plotting the pressure drop versus the flow rate gives the conductance of the nanolith. The curves for oxygen and helium plotted in Fig. 8 are linear in the pressure range 1.0–5.0 psi. The conductance measured from the slope of the linear fitting for helium (0.235 sccm/s/psi) is nearly three times that measured for oxygen (0.078 sccm/s/psi). Both lines extrapolate close to 0 sccm/s at 0 psi, with a small intercept of 0.04 sccm/s for helium flow and 0.02 sccm/s for oxygen. The nonzero intercepts are likely due to uncertainty in the absolute calibration of the pressure gauge. Detailed analysis of the gas flow through these nanopores and its relation to the pore size has been discussed elsewhere (Stair et al., 2006; Albo et al., 2006).

To check the mechanical and structural stability of the AAO structure under the conditions of catalytic reaction, the sealed nanolith was heated to 500 °C for several hours in flowing oxygen. After the test, no leak from the fitting was detected, and no cracks were found either on the AAO structure or at the AAO/aluminum boundaries by SEM. In our experience a 70-μm thick nanolith can withstand a pressure difference as high as 11 psi.

A most remarkable feature of the nanolith catalytic system is that the reactants must flow through the nanopores in the AAO structure, which makes each of these pores function as a nanoscale reactor. The surface area of the AAO measured by the B.E.T. method agrees with that calculated from the SEM imaging results, consistent with the absence of micro-pores in the nanolith walls (Crawford et al., 1992). Since the nanopore in the AAO has the shape of a long straight tube, it is natural to view each pore in relation to a plug flow reactor. However, because the dimensions of these nanoreactors are so small, diffusion also has to play an important role in the mass transfer. A plug flow with dispersion model may be appropriate for analyzing the mass transfer (Levenspiel, 1997). In an elementary section of the nanopore pictured in Fig. 9, if u denotes the linear velocity of the reactant flow (m/s), C_A is the concentration of the reactant, x

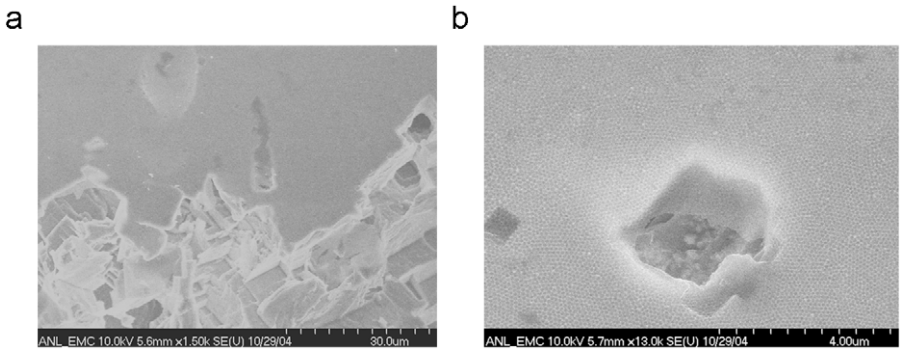

Fig. 4. SEM pictures of the AAO/aluminum boundaries on the front (anodized) side. (a) The AAO/aluminum interface. The flat layer in the upper part of the picture is the AAO. (b) A defect point (a pit) in the AAO near the interface. Aluminum is visible under a very thin layer of AAO.

Author's personal copy

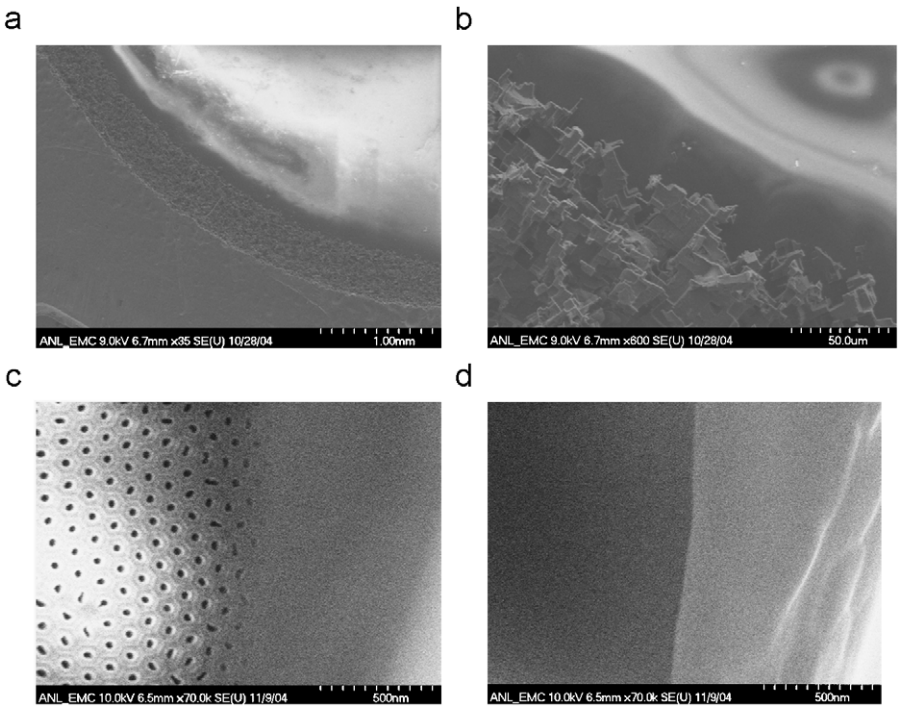

Fig. 5. SEM pictures of the AAO/aluminum boundaries on the back (etched) side. (a) The AAO/aluminum interface (low magnification). (b) The AAO/aluminum interface. High magnification pictures of the interface when the beam is focused on the AAO (c) and aluminum (d).

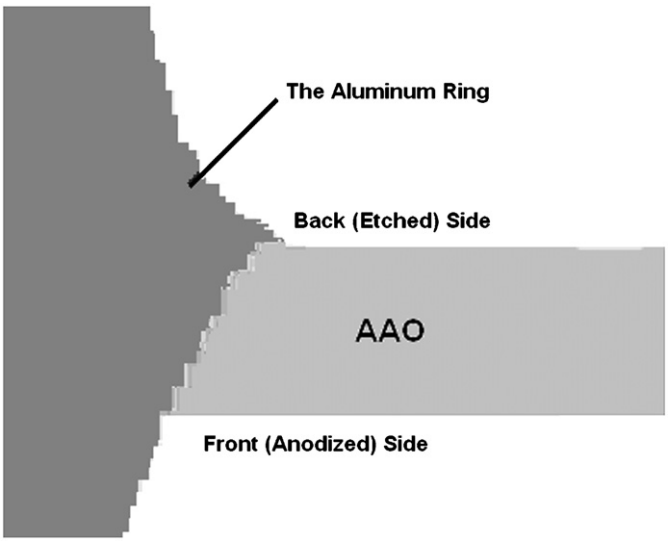

Fig. 6. The configuration of the AAO/aluminum connection. The jagged edges represent the rough boundaries generated by anodization (on the front side) and etching (on the back side) of aluminum as is shown in Figs. 4 and 5.

or l denotes the length of the tube, S is the cross-sectional area of the channel, d is the diameter of the nanopore, D is the diffusion constant (m^2/s), and k is the chemical reaction rate constant, the mass balance equation is expressed as

$$u\left(\frac{dC_A}{dl}\right) - D\left(\frac{d^2C_A}{dl^2}\right) + k'C_A = 0\left(k' = \frac{4k}{d}\right) \tag{1.1}$$

The three terms in Eq. (1.1) represent the contributions from mass flow, diffusion and chemical reaction, respectively. In this equation the chemical reaction is considered a first order reaction, whose rate is proportional to the concentration of the hydrocarbon reactant.

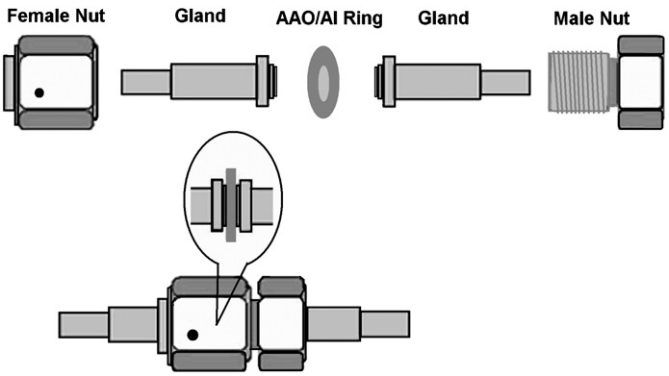

Fig. 7. The nanolith sealed in a VCR fitting as a gasket.

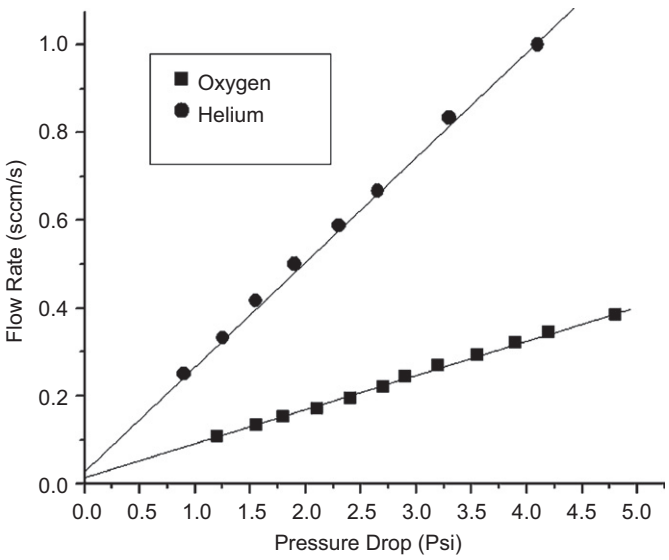

Fig. 8. The conductance of the nanolith measured with oxygen and helium.

Author's personal copy

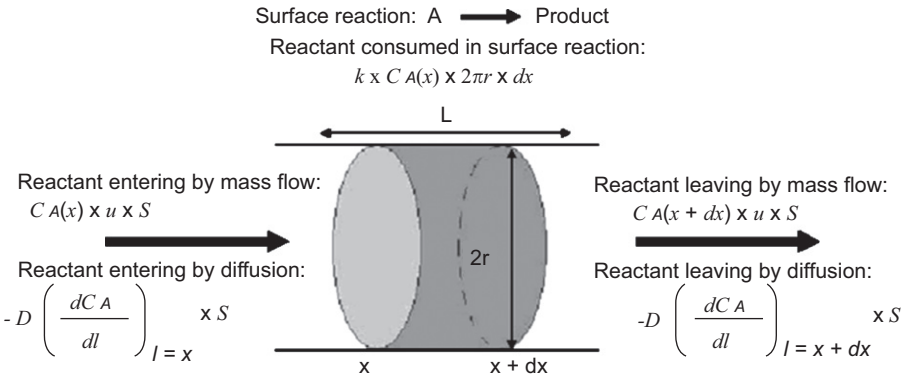

Fig. 9. The mass balance in an elementary section of the nanopore. The parameters are defined in the text.

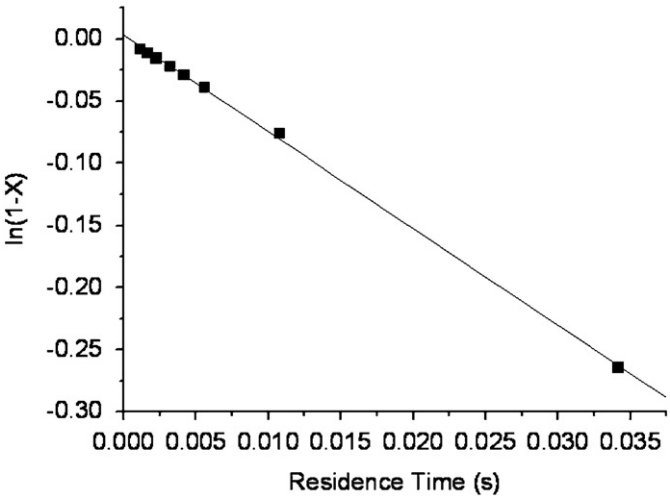

Fig. 10. Ln(1−X) versus residence time plot, where X is the conversion. The linear correlation indicates a first order reaction.

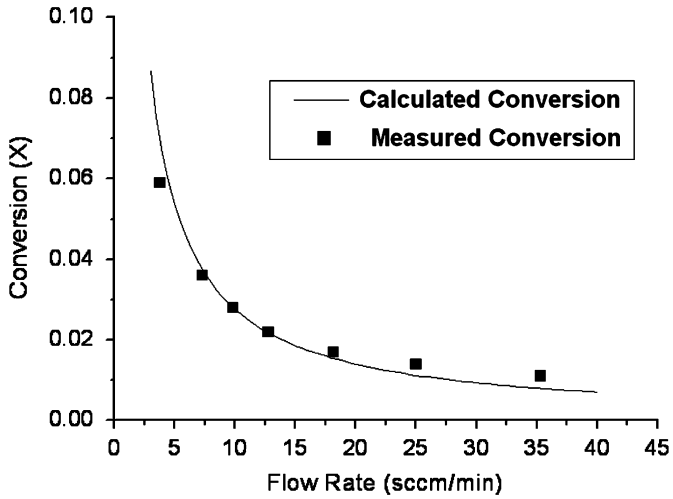

Fig. 11. Comparison of calculated and measured conversions as a function of reactant flow rate.

Catalytic ODH of cyclohexane, experiments have been carried out at different concentrations of cyclohexane and oxygen on a 2-cycle VO_x ALD coated nanolith. The results indicate that this reaction is overall first order since the measured rate (conversion) is proportional to the concentration of cyclohexane and nearly independent of oxygen concentration. Additional proof of the first order behavior of this reaction is obtained by measuring the conversions at different residence times. These measurements were taken by changing the flow of balance gas through the nanolith reactor. In these tests the conversion (X) shows a typical exponential correlation to the residence time. The logarithm of (1−X) versus residence time (L/u) is seen to be linear as shown in Fig. 10 .

In dimensionless form where $z = l/L$, $\tau = L/u$ (the residence time), the above equation becomes

$$\frac{D}{uL}\left(\frac{\mathrm{d}^2C_A}{\mathrm{d}z^2}\right) - \frac{\mathrm{d}C_A}{\mathrm{d}z} - k'\tau CA = 0 \tag{1.2}$$

In this equation, the coefficient of the first term D/uL determines the contribution from diffusion to the reactor performance or how much the system deviates from the plug flow model. When the D/uL value is small enough (< 0.01), the reactor is very similar to a plug flow reactor; while its performance transforms to more of a mixed flow reactor as the D/uL value becomes larger. In the nanopores of the AAO structure where the mean free path of the reactant molecule is much longer than the diameter of the pores, Knudsen diffusion is the predominant diffusion mode (Albo et al., 2006). The Knudsen diffusion constant can be estimated as (Malek and Coppens, 2003)

$$D_k = \frac{2}{3}r\sqrt{\frac{8RT}{\pi M}} \tag{1.3}$$

where r is the radius of the pore and M is the molar mass of the molecule. In most of our experiments ($T = 673$–753 K, $v = 10$ sccm/min), the D_k value is estimated to be approximately 1.1×10^{-5} m^2/s, and the corresponding D/uL coefficient is approximately 4.9. This D/uL value implies that Knudsen diffusion makes a significant contribution to the mass transfer in the nanopores, therefore a large deviation from the plug flow model is expected. The nanolith is very likely to function more like a mixed flow reactor rather than a plug flow reactor.

Since the performance of the nanolith can be expressed by Eq. (1.2), the conversion of the reactant passing through the catalytic nanolith structure at different flow rates (u) can be estimated by solving the differential equation once the reaction constant k is determined. For cyclohexane ODH on a nanolith coated with 1 ALD cycle of VO_x, the first order reaction constant k at 480 is calculated to be 6.93 s^{-1} from the conversion (2.8%) at a flow rate of 9.8 sccm/min. The conversions (X) at flow rates ranging between 3 and 40 sccm/min can be calculated by solving Eq. (1.2) and compared to the measured values as shown in Fig. 11. The agreement between measured and calculated conversions is very good. At very

Author's personal copy

Table 1
Comparison of the catalytic performance between a sealed, intact nanolith, and a powdered nanolith

T (°C)	Nanolith					Powder				
	Conversion (%)	Selectivity (%)				Conversion (%)	Selectivity (%)			
		C_6H_{10}	C_6H_6	CO	CO_2		C_6H_{10}	C_6H_6	CO	CO_2
400	1.00	54.6	26.6	1.7	16.9	0.92	30.7	36.1	6.4	26.7
420	1.67	49.6	35.5	3.2	11.8	1.18	28.0	38.2	10.6	23.2
450	3.48	38.0	46.0	3.6	12.4	2.40	21.4	46.2	10.2	27.5
465	4.79	33.3	51.3	4.5	10.9	3.35	17.6	49.1	10.9	22.4
480	6.35	28.6	54.7	5.3	11.4	4.52	15.2	50.5	11.0	23.3

low flow rates the observed deviation is likely due inaccuracy in the flow control by the mass flow controller. This analysis shows that the performance of these nanoreactor arrays can be predicted using the mixed flow model and controlled by adjusting the experiment settings.

The performance of the nanolith catalytic system and a conventional powder bed for the ODH of cyclohexane was compared by conducting the reaction on an intact nanolith sealed in the VCR flow reactor and on the same material crushed into a powder. In a previous comparison nanolith and powder catalytic materials were separately prepared (Stair et al., 2006). However, in that study it was not possible to test materials with the same alumina support (amorphous ALD versus crystalline transition alumina) or the same vanadium surface density and uniformity. The samples used in present experiments were prepared by coating the AAO structure with two ALD cycles of VO_x. The surface areas calculated from the SEM-measured pore density and pore diameter and measured by BET are in agreement, giving a value of 0.05 m^2. The vanadium density calculated from the surface area and the vanadium content measured by ICP is 3.7 V/nm^2. Catalytic results from multiple experiments are reproducible with no evidence of deactivation. After these tests the nanolith was ground into a fine powder and mechanically mixed with SiC, an inert diluent used to increase the total volume of the catalytic layer. Since ALD produces an extremely even dispersion of the catalytic species, VO_x particles are not formed on the surface of the AAO structure. This means that the process of grinding the AAO into a powder should not change the structure or chemical properties of the VO_x catalyst or the number of the active sites. The powder mixture was loaded into the VCR flow reactor to produce a catalyst bed approximately 1 mm thick. The powders were pushed firmly from both sides by quartz wool to form a densely packed layer and minimize bypass around the catalyst bed. The catalytic reaction was performed under the same experimental conditions used for the intact nanolith. The results from the nanolith and the powder bed are compared in Table 1.

The results in Table 1 show that the conversion and selectivity of the two systems share some common features. As the conversion increases with reaction temperature, the selectivity to cyclohexene decreases while the selectivity to benzene increases. These trends reflect a typical hydrocarbon sequential oxidation pathway in which the alkane is first oxidized to the alkenes and then further oxidized to the more stable products. On the other hand, a much better selectivity to cyclohexene is achieved with the nanolith system as compared to the powder bed despite comparable or slightly higher conversions with the nanolith. With the sealed nanolith, the selectivity to the deep oxidation products, CO and CO_2, is relatively low and independent of reaction temperatures and conversions. In contrast, a much larger fraction ($\sim 2X$) of the reactant is converted to CO_x over the powder catalyst. The selectivity to benzene is similar in the two configurations. These results are consistent with the results reported in Stair et al. (2006), and demonstrate that the differences in catalyst material in the earlier study were not responsible for the changes in catalytic performance.

We believe that the lower selectivity to CO_x is due to an inhibition of gas phase reactions by the nanolith compared to the powder. Since the selectivity toward benzene and CO_x are uncorrelated (as opposed to cyclohexene and benzene which are highly correlated), it appears that CO_x is formed directly from cyclohexane or cyclohexene rather than by a consecutive path through benzene as an intermediate. The production of CO_x can result from surface-activated homogeneous reactions initiated by desorption of reactive intermediates from the catalytic surface. These intermediates may be in the form of alkyl radicals that react with molecular oxygen in the gas phase (Sinev et al., 1995). The gas phase reactions will mainly take place in the void volumes of the catalytic layer since other spaces of the reactor have been filled with quartz chips, which have been shown to effectively quench free radicals and inhibit homogeneous reactions (Kung, 1994). In the pores of the nanolith, because the diameter of the nanopores is less than the mean free path of the reactant molecules, collisions between the reactant molecules and the pore walls are much more frequent than collisions between gas phase reactants. The potential for homogeneous free radical reactions can be effectively quenched due to readsorption or radical transfer processes at the pore walls. The gas phase reactions will occur primarily in the regions close to the pore openings where free radicals can escape the pores and quenching is less efficient. By grinding the AAO into a fine powder the number of pore openings is significantly increased along with the contribution from gas phase reactions.

It appears that the nanolith has similar but somewhat higher activity compared to the powder bed at reaction temperatures above 400 °C. One possible explanation is that the contact between reactant and catalyst is enhanced in the nanolith system. To evaluate the likelihood of this possibility, the effectiveness factors of the two systems are compared. From the values of the diffusion constant and the measured reaction rate coefficient (see above) and the size and shape of the nanopores, the calculated effectiveness factors of the nanolith and the powder bed systems are both essentially one (1). It does not appear that the small difference in observed activities is due to an internal diffusion effect. A more likely cause is the technical difficulty in reproducing exactly the same reaction conditions in the two experiments. For example, because of the extremely small amount of catalyst employed, it was not possible to verify by direct measurement that the catalyst material had the same temperature profile in the two experiments. For the same reason it was not possible to eliminate the possibility of reactant by-pass in the powder bed system. In view of these difficulties the agreement in measured conversion is quite good. In any case these factors are not responsible for the remarkably lower selectivity to CO_x observed with the nanolith even at a higher conversion than the powder.

4. Conclusions

AAO structures have been successfully mounted in an aluminum ring support by forming the AAO in the center of an aluminum disc. The structure connects seamlessly to the aluminum ring so that an air-tight seal can be formed between the nanolith and a conventional flow reactor by using the aluminum ring as a gasket in a standard

Author's personal copy

Swagelok VCR fitting. The straight nanopores on the AAO structure function as an array of nanoreactors. Attaching catalysts to the walls of the nanopores turns the AAO structure into a nanolith catalytic system. These catalytic nanoliths are stable up to a pressure differential of 11 psi at temperatures up to 550 °C.

Both mass flow and diffusion contribute to the mass transfer through nanopores in the AAO structure. For the dimensional scale of these nanopores, Knudsen diffusion is the predominant transport mode. The Knudsen diffusion constant can be estimated and compared to the mass flow factor. The result shows that mass transfer inside these nanopores is close to the mixed flow model. Theoretical estimation on the performance of the nanolith system was made based on a simple plug flow with dispersion model. The estimated conversions at different reactant flow rates are in agreement with the experimental data.

The ODH of cyclohexane catalyzed by supported vanadium oxide in the nanolith catalytic system has been compared to the same material prepared as a conventional powder bed. The nanolith system has demonstrated higher selectivity to the partial oxidation product at similar conversions as compared to the powdered nanolith system. These results show that the nanolith effectively reduces homogeneous reactions, which lead to the formation of CO_X, as a result of free radical quenching inside the nanopores.

Acknowledgments

The work at Argonne is supported by the US Department of Energy, BES-Materials Sciences (materials synthesis), and BES-Chemical Sciences (catalytic activity) under Contract W-31-109-ENG-38. The work at Northwestern is supported by the US Department of Energy, BES-Chemical Sciences, Geosciences and Biosciences Division under Grant no. DE-FG0203ER15457. The electron microscopy was performed at the Electron Microscopy Center for Material Research at Argonne National Laboratory.

References

Albo, S.E., et al., 2006. Multiscale modeling of mass transport and residence times in nanostructured membranes. A.I.Ch.E. Journal 52, 3679–3687.
Corberan, V.C., 2005. Novel approaches for the improvement of selectivity in the oxidative activation of light alkanes. Catalysis Today 99, 33–41.
Crawford, G.P., et al., 1992. Characterization of the cylindrical cavities of anopore and nuclepore membranes. Journal of Chemical Physics 96 (10), 7788–7796.
Elam, J., et al., 2002. Viscous flow reactor with quartz crystal microbalance for thin film growth by atomic layer deposition. Review of Scientific Instruments 73, 2981–2987.
Gao, T., et al., 2002. Template synthesis of Y-junction metal nanowires. Journal of Applied Physics A 74, 403–406.
Goodwin, J.G., et al., 2004. Turnover frequencies in metal catalysis: meanings, functionalities, and relationships. Catalysis 17, 320–347.
Keranen, J., et al., 2004. Preparation by atomic layer deposition and characterization of active sites in nanodispersed vanadia/titania/silica catalysts. Catalysis Today 91–92, 67–71.
Kung, H.H., 1994. Oxidative dehydrogenation of light (C2 to C6) alkanes. Advances in Catalysis 40, 1–23.
Kuo, T., Xu, J., 2006. Growth and application of highly ordered array of vertical nanoposts. Journal of Vacuum Science & Technology B 24, 1925–1933.
Kyotani, T., et al., 2002. Chemical modification of carbon-coated anodic alumina films and their application to membrane filter. Journal of Membrane Science 196, 231–239.
Li, J., et al., 1999. Nanoelectronics: growing Y-junction carbon nanotubes. Nature 402, 253–254.
Levenspiel, O., 1997. Chemical Reaction Engineering, third ed., p. 312.
Malek, K., Coppens, M.O., 2003. Knudsen self- and Fickian diffusion in rough nanoporous media. Journal of Chemical Physics 119, 2801–2811.
Mamedov, E.A., Corberan, V.C., 1995. Oxidative dehydrogenation of lower alkanes on vanadium oxide-based catalysts: the present state of the art and outlooks. Applied Catalysis A 127, 1–40.
Martin, C.R., 1994. Nanomaterials: a membrane-based synthetic approach. Science 266, 1961–1966.
Masuda, H., Fukuda, K., 1995. Ordered nanohole arrays made by two-step replication of honeycomb structures of anodic alumina. Science 268, 1466–1467.
Masuda, H., et al., 1997. Highly ordered nanochannel-array architecture in anodic alumina. Applied Physics Letters 71, 2770–2772.
McCormick, J.A., et al., 2007. Quantities of nanoparticles. Journal of Vacuum Science & Technology A 25, 67–74.
Panizza, M., et al., 2003. A study of the oxidative dehydrogenation of cyclohexane over oxide catalysts. Catalysis Letters 89, 199–205.
Patermarakis, G., Pavlidou, C., 1994. Catalysis over porous anodic alumina catalysts. Journal of Catalysis 147, 140–155.
Roy, S., et al., 2003. Modeling gas flow through microchannels and nanopores. Journal of Applied Physics 93, 4870–4879.
Sinev, M.Y., et al., 1995. Heterogeneous free-radical reactions in oxidation processes. Russian Chemical Reviews 64, 349–364.
Stair, P., et al., 2006. Novel, uniform nanostructured catalytic membranes. Topics in Catalysis 39, 181–186.
Tomioka,T., Yoshida, A., 2001. Anti-microbial aluminum product and method for producing the same. US Patent 6168869.
Weitkamp, J., et al., 1999. Catalysis and Zeolites, pp. 327–376.